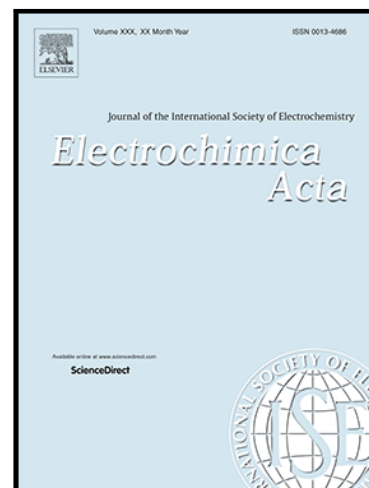


Journal Pre-proof

A novel composite electrode material derived from bisferrocenyl-functionalized GO and PANI for high performance supercapacitor

Elmira Payami , Reza Teimuri-Mofrad , Iraj Ahadzadeh ,
Reza Mohammadi

PII: S0013-4686(20)31105-1
DOI: <https://doi.org/10.1016/j.electacta.2020.136712>
Reference: EA 136712



To appear in: *Electrochimica Acta*

Received date: 28 March 2020
Revised date: 29 June 2020
Accepted date: 1 July 2020

Please cite this article as: Elmira Payami , Reza Teimuri-Mofrad , Iraj Ahadzadeh , Reza Mohammadi , A novel composite electrode material derived from bisferrocenyl-functionalized GO and PANI for high performance supercapacitor, *Electrochimica Acta* (2020), doi: <https://doi.org/10.1016/j.electacta.2020.136712>

This is a PDF file of an article that has undergone enhancements after acceptance, such as the addition of a cover page and metadata, and formatting for readability, but it is not yet the definitive version of record. This version will undergo additional copyediting, typesetting and review before it is published in its final form, but we are providing this version to give early visibility of the article. Please note that, during the production process, errors may be discovered which could affect the content, and all legal disclaimers that apply to the journal pertain.

© 2020 Elsevier Ltd. All rights reserved.

A novel composite electrode material derived from bisferrocenyl-functionalized GO and PANI for high performance supercapacitor

Elmira Payami^{a,b}, Reza Teimuri-Mofrad^{a,*}, Iraj Ahadzadeh^b, Reza Mohammadi^a

^a Department of Organic and Biochemistry, Faculty of Chemistry, University of Tabriz, Tabriz, Iran

^b Department of Physical Chemistry, Faculty of Chemistry, University of Tabriz, Tabriz, Iran

Corresponding author: Tel.: +98 413 339 3105; Fax: +98 413 334 0191;

E-mail address: teymouri@tabrizu.ac.ir (Reza Teimuri-Mofrad)

Credit author statement

Elmira Payami: Investigation, Writing-Original draft preparation, Conceptualization, Methodology, Software, **Reza Teimuri-Mofrad:** Supervision, **Iraj Ahadzadeh:** Validation, Reviewing and Editing, **Reza Mohammadi:** Visualization.

Abstract

A novel bisferrocenyl based epoxy compound was synthesized to be used for further surface modification of graphene oxide (GO). GO surface was firstly modified with ethylenediamine (EDA) as an amine linker and then bisferrocenyl based epoxy compound was covalently grafted to the GO surface through the epoxide ring opening reaction. Afterwards, polyaniline (PANI) nanofibers were physically adsorbed onto the surface of the modified GO to obtain a potentially high-performance nanocomposite for battery-type supercapacitor applications. The surface modification, crystalline structure, morphology, composition, and microstructure of the synthesized nanocomposites were further investigated using Fourier transform infrared spectroscopy (FT-IR), X-ray diffraction (XRD), field emission scanning electron microscopy (FESEM), energy dispersive X-ray (EDX) and N₂ adsorption/desorption analyses, respectively. Also, the electrochemical behavior of the synthesized nanocomposites was investigated by electrochemical methods of cyclic voltammetry (CV), electrochemical impedance spectroscopy (EIS), galvanostatic charge-discharge measurement (GCD). The final nanocomposite electrode exhibited a charge storage capacity of 272 mAh g⁻¹, and capacity retention of 89 % over 3000 CV cycles. A high energy density of 69.3 Wh kg⁻¹ and high power density of 6171 W kg⁻¹ were achieved in a symmetrical two-electrode configuration.

Keywords: Ferrocenyl based compound, Polyaniline, Battery-type supercapacitor, Nanocomposite.

1. Introduction

Supercapacitors are among the most important energy storage and conversion systems that have attracted the attention of related scientific society in recent decades. The important features and advantages of supercapacitors over other energy storage systems are as follows: high power density, superior durability, low maintenance cost, safety, and fast charge/discharge rate [1-3]. Depending on the charge storage mechanism, supercapacitors are divided into two different classes: an electrostatic attraction as in electrical double layer capacitors (EDLCs) and battery-type faradic redox reaction in pseudocapacitors [4, 5]. EDLCs store charge using electrostatic attraction of electrolyte ions between the electrode/electrolyte interface (Helmholtz layer), whereas pseudocapacitors store energy via fast faradaic redox reaction of the electroactive compounds such as ferrocene (Fc), transition metal oxide, and conductive polymers on the active electrochemical sites with electrolyte [6-10]. Graphene, activated carbon, carbon nanotubes are the materials used in EDLCs. Among these carbon allotropes, graphene is one of the most promising candidates for use in the electrode materials because of its prominent properties including large surface area, high conductivity, excellent mechanical and chemical stabilities, and low cost [11-15]. Despite these outstanding features, graphene-based electrode shows low capacitance due to the limited exploitation of large surface area; therefore, its use in pure state is not suitable for supercapacitor applications [16]. Unlike carbon based materials, the pseudocapacitive compounds such as conductive organic polymers including PANI [17, 18], polypyrrole (PPY) [19-22], and polythiophene (PTh) [23, 24], and some common transition metal oxides (mostly V_2O_5 , MnO_2 , RuO_2 , and metal sulfides) exhibit superior capacitive behavior compared to EDLCs due to their rather fast reversible faradaic redox reactions [25, 26]. Among the various conductive polymers, PANI as one of the typical conductive organic

polymers is the best candidate for supercapacitor applications because of its low cost, high pseudocapacitance, good environmental stability [27-29]. PANI despite its unique features often suffers from poor cycling stability and rate capability. Many attempts have been taken to modify the performance of the PANI. One of these approaches is the synthesis of PANI with various structures such as nanowires, nanorods, nanotubes or nanofibers, which improves the surface area and electrolyte ion diffusion and consequently improves the capacitance and rate capability compared to the intact PANI. Synthesis of PANI nanocomposites with various carbon based materials such as graphene oxide, carbon nanotube, and amorphous carbon is another way to improve the properties of PANI. The synergistic effects between PANI and carbon based materials lead to larger capacitance, good rate capability, and cycle durability [30-33].

Organometallic compounds exhibit good optoelectronic properties due to their electron delocalization and therefore received much attention of scientists. Among the organometallic materials ferrocene (Fc) due to its unique features such as superior redox reversible properties, high stability, and non-toxicity can be applied in various fields such as electrocatalysis, electroanalysis, and biosensors [34, 35]. Modification of GO nanosheets with ferrocenyl based compounds can be improved the electrochemical properties of the GO [36-40].

In general, hybridizing the battery-type and EDLCs-type electrode materials provide many significant advantages and improvements in the performance of the electrochemical properties compared to their individual components. Modified GO was prepared via two different methods including non-covalent and covalent functionalization approaches. In the case of non-covalent interaction, modified GO nanosheets were prepared via a strong π - π electronic interaction between GO layers and other appropriate materials. In the former functionalization method, the

active oxygenic groups on the GO surface play an important role in the covalently grafting of electroactive materials onto GO surfaces [41].

In this work, a novel bisferrocenyl based epoxy compound was synthesized, investigated via some analysis, and then this synthesized electroactive compound was covalently grafted onto GO surfaces through ring-opening reaction. The PANI nanofibers was then treated with modified GO to obtain a novel Fc-based nanocomposite. Furthermore, various analyses methods were employed to investigate the structural and electrochemical properties of the synthesized nanocomposite. The final nanocomposite exhibits good electrochemical performance. The enhancement in electrochemical performance of the final nanocomposite can be attributed to the synergistic effects between both battery-type components including Fc and PANI nanofiber and EDLCs-type component including GO nanosheets.

2. Experimental section

2.1. Materials

All of materials used during synthesis processes are given below:

α -acetyl- γ -butyrolactone, hydrochloric acid (HCl), sulfuric acid 98% (H₂SO₄), sodium acetate, sodium iodide (NaI), potassium carbonate (K₂CO₃), epichlorohydrin (ECH), sodium hydroxide pellets (NaOH), tetrabutylammonium iodide (Bu₄NI), dimethylformamide (DMF), methanol (MeOH), graphite flake, potassium permanganate (KMnO₄), sodium nitrate (NaNO₃), hydrogen peroxide (H₂O₂), EDA, potassium hydroxide pellets (KOH), *p*-toluenesulfonic acid (PTSA), toluene, aniline (double-distilled before use), ammonium persulfate (APS). All other materials were of analytical grade and were used without any further purification.

2.2. Synthesis procedures

2.2.1. Preparation of ethylferrocene (EtFc)

EtFc was prepared according to our previously reported procedure [42].

2.2.2. Preparation of 5-chloro-2-pentanone

A mixture of 12 ml conc. HCl, 14 ml H₂O, and 10 g (78.13 mmol) α -acetyl- γ -butyrolactone were placed in a two necked distilling flask equipped with a condenser and the receiver was immersed in an ice-bath. The entire reaction vessel was quickly immersed into the oil bath preheated at 100 °C. After about 10 min the color was changed from yellow to orange and then to black. After 20 ml of distillate have been collected, 7 ml H₂O was added to the distilling flask and another 5 ml of distillate was collected. Afterwards, the yellow organic layer was separated and the aqueous layer was extracted with dichloromethane and dried over Na₂SO₄, and the solvent was evaporated. An amount of 6 g 5-chloro-2-pentanone was obtained as yellow, viscous oil in 64 % yield [43].

2.2.3. Synthesis of 5-chloro-2,2-bis(ethylferrocenyl)pentane (BisFc-Cl)

A 50 ml, two necked flask equipped with a dropping funnel and gas inlet tube was charged with a 5 ml H₂SO₄ and 5 ml dry MeOH, this mixture was stirred for 24 h at room temperature. After this time, EtFc (26 mmol, 5.58 g) and 5-chloro-2-pentanone (13 mmol, 1.5 ml) were slowly added into the reaction flask and were stirred at 65 °C for 30 h. After completion of the reaction (controlled by TLC), the reaction mixture was cooled slowly to room temperature and was neutralized with aqueous sodium carbonate, then extracted with dichloromethane (3×30 ml) and dried over anhydrous Na₂SO₄. After the solvent removal, the crude product was purified by column chromatography (n-hexane). BisFc-Cl was obtained as brown-orange viscous oil in 60% yield [44].

FT-IR (KBr): 3090 (Ar-H), 2964, 2871 (C-H), 1640, 1454 (C=C), 483 (C-Fe); ^1H NMR (400 MHz, CDCl_3): δ 1.09-1.19 (6H, m, $\text{CH}_2\text{-CH}_3$), 1.55-1.67 (5H, m, $-\text{CH}_3$, C- CH_2), 1.92-2.01 (2H, m, C- $\text{CH}_2\text{-CH}_2$), 2.24-2.37 (4H, m, Cp- CH_2), 3.43-3.47 (2H, m, $\text{CH}_2\text{-Cl}$), 3.84-4.10 (16H, m, Cp) ppm.

2.2.4. Synthesis of 5-acetoxy-2,2-bis(ethylferrocenyl)pentane (BisFc-OAc)

To a solution of BisFc-Cl (0.1 g, 0.19 mmol) in 2 ml DMF were added sodium acetate (0.05 g, 0.57 mmol) and NaI (0.3 g, 0.19 mmol) and this solution was heated to 120 °C overnight. After this time period, the reaction mixture was cooled down to room temperature then partitioned between water and dichloromethane. The organic layer was washed several times with water, dried over anhydrous Na_2SO_4 , and the solvent was evaporated. The crude product was purified by column chromatography 9:1 (n-hexane-ethyl acetate) to afford BisFc-OAc as brown-orange viscous oil in 94% yield [45].

FT-IR (KBr): 3090 (Ar-H), 2964 (C-H), 1737 (C=O), 1646, 1456 (C=C), 1239 (C-O), 484 (C-Fe); ^1H NMR (400 MHz, CDCl_3): δ 1.09-1.19 (6H, m, $\text{CH}_2\text{-CH}_3$), 1.49-1.62 (5H, m, $-\text{CH}_3$ and C- CH_2), 1.86-1.91 (2H, m, C- $\text{CH}_2\text{-CH}_2$), 2.04 (3H, s, (C=O) CH_3), 2.25-2.35 (4H, m, Cp- CH_2), 3.92-4.10 (18H, m, O- CH_2 and Cp) ppm.

2.2.5. Synthesis of 4,4-bis(ethylferrocenyl)pentanol (BisFc-OH)

To a solution of BisFc-OAc (0.53 g, 0.96 mmol) in MeOH (40 ml) was added K_2CO_3 (1.41 g, 10.27 mmol). This suspension was stirred at room temperature for 2 h. Afterwards the reaction mixture was diluted with distilled water and extracted with dichloromethane (3×10 ml). The combined organic layers were dried over anhydrous Na_2SO_4 and the solvent was concentrated to afford BisFc-OH as brown-orange viscous oil in 100% yield [46].

FT-IR (KBr): 3382 (OH), 3090 (Ar-H), 2963, 2872 (C-H), 1641, 1455 (C=C), 483 (C-Fe); ^1H NMR (400 MHz, CDCl_3): δ 1.08-1.18 (6H, m, $\text{CH}_2\text{-CH}_3$), 1.47-1.48 (2H, m, C- CH_2), 1.57-1.63 (4H, m, $-\text{CH}_3$ and OH), 1.81-1.90 (2H, m, C- $\text{CH}_2\text{-CH}_2$), 2.24-2.37 (4H, m, Cp- CH_2), 3.54-3.56 (2H, m, $\text{CH}_2\text{-OH}$), 3.90-4.07 (16H, m, **Cp**) ppm.

2.2.6. Synthesis of 2-[(4,4-bis(ethylferrocenyl)pentoxy)methyl]oxirane (BisFc-Epo)

A 25 ml, two necked round bottom flask equipped with dropping funnel and condenser was charged with BisFc-OH (0.72 g, 1.4 mmol), NaOH (0.08 g, 2.05 mmol), and a catalytic amount of Bu_4NI (as a phase transfer catalyst). ECH (0.2 g, 2.1 mmol) was added dropwise to the mixture and stirred at 30 °C for 48 h. After two days, the reaction mixture was diluted with water and extracted with dichloromethane (3×10 ml). The combined organic layers were dried over anhydrous Na_2SO_4 and after the solvent was evaporated, the crude product was purified with column chromatography 9:1 (n-hexane-ethylacetate) to afford BisFc-Epo as brown-orange viscous oil in 75% yield [39].

FT-IR (KBr): 3089 (Ar-H), 2955 (C-H), 1644, 1458 (C=C), 482 (C-Fe); ^1H NMR (400 MHz, CDCl_3): δ 1.08-1.18 (6H, m, $\text{CH}_2\text{-CH}_3$), 1.39-1.51 (2H, m, C- CH_2), 1.57-1.62 (3H, m, $-\text{CH}_3$), 1.78-1.90 (2H, m, C- $\text{CH}_2\text{-CH}_2$), 2.23-2.36 (4H, m, Cp- CH_2), 2.58-2.61 and 2.76-2.79 (2H, m, CH_2 epoxide), 3.10-3.13 (1H, m, $-\text{CH}$ - epoxide), 3.32-3.43 (3H, m, $-\text{O-CH}_2\text{-CH-CH}_2$ and $-\text{CH}_2\text{-CH}_2\text{-O-}$), 3.62-3.67 (1H, m, $-\text{CH}_2\text{-CH}_2\text{-O-}$), 3.90-4.05 (16H, m, **Cp**) ppm.

2.2.7. Preparation of PANI

PANI was prepared chemically by an interfacial polymerization method according to the literature [47].

2.2.8. Preparation of GO

The GO product was prepared from graphite using Hummers method [48]. In brief, pristine graphite (5 g), NaNO_3 (2.5 g), and 130 ml conc. (98%) H_2SO_4 was placed into a 2-liter round bottomed flask. This mixture was vigorously stirred for 1 h at 0 °C. After that, 15 g KMnO_4 was slowly added to the above mixture and stirred for 72 h at room temperature. As the reaction progressed, the dark color of the mixture was changed to light brown. Then, 350 ml distilled water was slowly added to the mixture and after the mixture was cooled to 25 °C, 60 ml H_2O_2 (30%) and 200 ml HCl (10%) solution was added into the flask, respectively. Finally, the GO product was obtained after centrifuging/washing process (with HCl (5%) and water). After freeze-drying, the GO nanosheets were obtained as a brownish powder.

2.2.9. Modification of GO with ethylenediamine (GO-EDA)

An amount of 200 mg of GO was added in 50 ml deionized water (DI) (4 mg/ml) and this mixture was exfoliated by ultrasonication till homogeneous dispersion was formed. Afterwards, 1 ml EDA was slowly added into this suspension under vigorous stirring. The suspension was stirred for 24 h at room temperature. After this time, the modified GO powder was centrifuged and washed several times with ethanol and DI water, respectively. The collected powder was dried in a vacuum oven at 60 °C [49].

2.2.10. Synthesis of chemical-functionalized of GO-EDA with Fc moiety (GO-EDA-BisFc)

An amount of 100 mg of GO-EDA was dispersed in 50 ml dry toluene for 30 min. A catalytic amount of PTSA and BisFc-Epo (300 mg) was added to this suspension and this mixture was refluxed for 24 h at 110 °C. At the end of the reaction, the solid powder was centrifuged at 1200 rpm and the obtained powder was thoroughly washed with DI water and dichloromethane,

respectively, until the filtrate became colorless followed by drying in a vacuum oven at 60 °C to obtain the GO-EDA-BisFc as a black powder [50].

2.2.11. Synthesis of GO-EDA-BisFc/PANI nanocomposite

An aqueous suspension of PANI (2 mg ml⁻¹) was added into the modified GO suspension in DI water (2 mg ml⁻¹) and the obtained mixture was stirred vigorously for 3 days at 25 °C. At the end, after centrifuging, the remaining precipitate was dried in a vacuum oven to gain the GO-EDA-BisFc/PANI nanocomposite.

2.3. Characterization techniques

The ¹H NMR data were collected on Bruker FT-400 spectrometers using TMS as an internal reference and CDCl₃ as a solution, respectively (The ¹H NMR spectra are given in the Supporting Information). FT-IR spectra were recorded using KBr disk on the Bruker-Tensor 270 spectrometer. The surface morphology, elementary composition, phase analysis, surface area and pore size were analyzed using FESEM (MIRA3 TESCAN), EDX spectroscopy (MIRA3 TESCAN) and XRD analysis (PANalytica X pertPRO (Germany)) with a Cu-K_α (λ = 1.5406 Å) radiation source, Brunauere-Teller (BET) (Belsorpmi II apparatus at 196 °C), and Barrete-Jovner-Halenda (BJH) (Belsorpmi II apparatus at 196 °C).

2.4. Electrochemical experiments

All electrochemical measurements were carried out in a conventional standard three electrode cell configuration: 2 μl of a mixture of 80 wt. % synthesized materials (GO, GO-EDA, PANI, GO-EDA-BisFc, and GO-EDA-BisFc/PANI nanocomposites), 10 wt. % carbon black and, 10 wt. % polyvinylidene fluoride in NMP was coated on a surface of carbon paper as the working electrodes, a platinum wire as an auxiliary electrode and an Ag/AgCl as the reference electrodes.

All of electrochemical measurements were performed in 1 M H₂SO₄ aqueous solution as a background electrolyte at room temperature. The electrochemical properties of GO, GO-EDA, PANI, GO-EDA-BiFc, and GO-EDA-BisFc/PANI nanocomposites were measured by CV (potential range of voltammograms between -0.2 to 0.8 V vs. Ag/Ag Cl), GCD and EIS spectroscopy (EG&G PARSTAT 2263).

3. Results and discussion

3.1. Synthesis and characterization of Fc-based epoxy compound (BisFc-Epo)

The synthesis procedures of the novel bisferrocenyl based epoxy compound are shown in scheme 1.

A coupling reaction between EtFc and 5-chloro-2-pentanone as a coupling agent in dry MeOH/H₂SO₄ leads to the formation of BisFc-Cl. Subsequently, BisFc-Cl was converted to the acetate form by treatment with sodium acetate in DMF at 120 °C, followed by the further hydrolysis of the acetate groups with methanolic K₂CO₃ in 2 h to afford BisFc-OH. Finally, BisFc-OH was reacted with epichlorohydrin in the presence of Bu₄NI as a phase transfer catalyst at 30 °C for 48 h and BisFc-Epo was obtained as a novel ferrocenyl based epoxy compound.

The ¹H NMR spectra of BisFc-Cl, BisFc-OAc, BisFc-OH, and BisFc-Epo in CDCl₃ are presented in Fig. S1. Also, the FT-IR spectra of the synthesized compounds were collected between 400 and 4000 cm⁻¹ and deposited as electronic supplementary information (see Fig. S2).

Electrochemical behaviors of the BisFc-Epo were investigated by the CV method (Fig. 1) that performed in a potential range of 0.0 to 0.8 V and 0.1 M LiClO₄ as a background supporting electrolyte. Two pairs of chemically reversible redox peaks were emerged on the CV curve in Fig. 3 that well separated together. These peaks were associated to the Faradic redox reaction of Fc/Fc⁺ redox couples.

3.2. Synthesis of functionalized GO with BisFc-Epo (GO-EDA-BisFc)

The preparation process of the functionalized GO is illustrated in scheme 2. As can be seen from the scheme 2, in the first step, the GO nanosheets were reacted with EDA as a linker in DI water. EDA as a nucleophile was attacked the epoxy rings on the GO nanosheets and opened them by ring opening reaction and the modified GO with EDA (GO-EDA) was formed. In the second step, the active NH_2 functional groups on the surface of the GO-EDA were reacted with the BisFc-Epo in the dry toluene. Then, the epoxy ring on the BisFc-Epo was opened and covalent bond was formed between the GO-EDA and BisFc-Epo.

3.3. Synthesis of GO-EDA-BisFc/PANI nanocomposite

After the functionalization of the GO nanosheets, both of the modified GO and neat PANI are physically combined to form the final nanocomposite (Scheme 3). There is the synergetic effect between modified GO nanosheets and neat PANI including hydrogen bonding, π - π stacking, and electrostatic interactions (Fig. 2) [51, 52].

The FT-IR spectra for the BisFc-Epo, GO, PANI, GO-EDA, GO-EDA-BisFc, GO-EDA-BisFc/PANI are shown in Fig. 3. As shown in the Fig. 3, in the FT-IR spectrum of BisFc-Epo the peak located at about 500 cm^{-1} can be attributed to Fe-C band in the Fc rings. The peaks at around 2900 and 3000 cm^{-1} can be related to the aliphatic and aromatic C-H stretching vibration, respectively. The peak at around 1640 cm^{-1} can be assigned to the C=C vibration of Fc rings and the peak at 1109 cm^{-1} can be attributed to the (C-O-C) in the epoxy ring. In the FT-IR of neat PANI, the well defined characteristic peaks corresponding to the quinoid and benzenoid rings were appeared at 1576 cm^{-1} and 1490 cm^{-1} , respectively [53, 54]. The absorption peak at about

1300 cm^{-1} can be assigned to the C-N stretching vibration band. The observed peaks at around 1100 cm^{-1} and 800 cm^{-1} can be attributed to the C-H in-plane bending vibration and the out-of-plane vibration, respectively [55]. The stretching vibration of N-H band was appeared at about 3400 cm^{-1} . These data confirmed the formation of neat PANI. For FT-IR spectrum of GO, the characteristic peaks were observed at about 3300 cm^{-1} , 1700 cm^{-1} , 1578 cm^{-1} , 1200 cm^{-1} , and 1050 cm^{-1} corresponding to the stretching vibration of O-H, C=O, C=C, C-O, and C-O-C bands, respectively [56]. In the FT-IR spectrum of the GO-EDA, the appearance of the new peaks at 1360 cm^{-1} , 2924 cm^{-1} , and 3400 cm^{-1} , which were respectively assigned to the stretching vibration of C-N, C-H, and N-H bands, indicating the successful modification of GO with EDA [57]. In the FT-IR spectrum of the GO-EDA-BisFc, a new peak at about 480 cm^{-1} was attributed to the Fe-C, which reflects the covalently-grafted of GO with BisFc-Epo compound. All characteristic peaks of the neat PANI and the GO-EDA-BisFc were appeared in the FT-IR spectrum of the final nanocomposite. The intensity some of oxygenated functional groups in the spectra of the GO-EDA-BisFc/PANI were reduced, which may be because of the reduction of these functional groups during the preparation of the final nanocomposite [58]. Finally, these findings proved that the final nanocomposite was successfully synthesized.

The surface morphology of the all of the synthesized compounds was analyzed using FESEM analysis. Fig. 4 illustrates the FESEM images of (a) PANI, (b) GO, (c) GO-EDA, (d) GO-EDA-BisFc, and (e & f) GO-EDA-BisFc/PANI nanocomposites. As demonstrated in Fig. 4a, the neat PANI was exhibited nanofibers type structure, which aggregated together. The FESEM image of GO nanosheets (Fig. 4b) showed the layered structure with lots of wrinkles and crumpled structure which can be related to the presence of various functional groups such as epoxy rings,

carboxylic acid, carbonyl and OH groups on the surface of GO nanosheets. The FESEM micrographs of the GO-EDA (Fig. 4c) showed the similar layered structure of GO, However, wrinkles on the surface have increased due to the modification of GO surface with EDA. As can be seen from the micrographs of GO-EDA-BisFc (Fig. 4d), after surface modification of GO with Fc groups the FESEM image of GO-EDA-BisFc showed the rough surface structure. The presence of PANI nanofibers in the final nanocomposite gives a microporous structure nanocomposite (Fig. 4e & 4f). Short diffusion length and high surface area between active materials and electrolyte ions as a result of such microporous structure suggested that the final nanocomposite can be applied in electrode materials for supercapacitor applications.

EDX analysis is an important method in order to investigate the elemental composition of the synthesized materials. The EDX curves of the (a) PANI, (b) GO, (c) GO-EDA, (d) GO-EDA-BisFc, and (e) GO-EDA-BisFc/PANI nanocomposite were illustrated in Fig. 5. As can be seen in Fig. 5c, the EDX pattern of GO-EDA reveals the presence of the N content in the modified GO nanosheets with EDA. The EDX spectrum of the GO-EDA-BisFc (Fig. 5d) confirmed the successful modification of GO surface with Fc moiety. The increasing of N and C contents in the EDX profile of the final nanocomposite (Fig. 5e) proved the coexistence of the PANI nanofibers and modified GO in the GO-EDA-BisFc/ PANI nanocomposite.

The phase composition and crystalline structure of the PANI, GO, GO-EDA, GO-EDA-BisFc, GO-EDA-BisFc/PANI were determined by XRD analysis and the related patterns were shown in Fig. 6. The XRD pattern of PANI exhibits rather low crystallinity attributable to the repetition of benzenoid and quinoid ring in the PANI chains [59, 60]. The sharp diffraction peak appeared at

$2\theta = 11.5^\circ$ can be assigned to the (001) crystal plane of GO. The value of the interlayer spacing of GO sheets depended on the oxygen functionality on the GO surface and the amount of adsorbed water layer [61]. Compared with GO, the (001) reflection peak of GO-EDA has been shifted to the lower angle ($2\theta = 10.5^\circ$) with an interlayer spacing of about 0.85 nm. These results essentially prove that a covalent bond is formed between GO sheets and EDA. As shown from the XRD pattern of GO-EDA-BisFc, modification of GO surface with BisFc-Epo compound has disrupted the layer structure of GO sheets and XRD pattern of GO-EDA-BisFc shows low crystallinity. The GO-EDA-BisFc/PANI exhibits all relevant related peaks of the composite components confirming the successful synthesis of the final nanocomposite.

Pore structure analysis of GO-EDA-BisFc and GO-EDA-BisFc/PANI nanocomposites were characterized by nitrogen adsorption-desorption BET isotherms at 77 K and the related diagrams were shown in Fig. 7. In both cases, diagrams showed a typical IV shape isotherm with a minor hysteresis loop at high pressures. These experimental results indicated that the GO-EDA-BisFc and GO-EDA-BisFc/PANI nanocomposites have almost mesoporous structure. According to data obtained from BET analysis, the GO-EDA-BisFc/PANI nanocomposite has a higher specific surface area ($16.82 \text{ m}^2 \text{ g}^{-1}$) and average pore diameter (28.3 nm) than GO-EDA-BisFc nanocomposite ($9.31 \text{ m}^2 \text{ g}^{-1}$), (22.0 nm), respectively. It can be concluded that incorporation of porous structure and large specific surface area increases the rate of diffusion of the electrolyte ions by reducing the diffusion path length from the bulk electrolyte to the active materials which further reflected as increased the electrochemical performance of as-prepared electrodes [62-64].

3.4. Electrochemical evaluations

Fig. 8a demonstrates the CV voltammograms of all of the as-prepared electrodes obtained at a scan rate of 50 mV/s in the potential range of -0.2 to 0.8 V. On the basis of the CV results,

voltammograms of the GO nanosheets and GO-EDA displays a similar rather rectangular shape due to the predominance of EDLC behavior in capacitance by the suitable surface charge storage. In the case of PANI, the presence of two redox peaks can be assigned to the redox process of PANI between the well-defined oxidation states: the leucoemeraldine form (semiconducting state) and polaronic emeraldine form (conducting state) [65]. Therefore, the PANI has a battery-type energy storage behavior. The CV curve of GO-EDA-BisFc showed a non-rectangular shape with a significant broad anodic and cathodic peaks, which can be assigned to the existence of the Fc core in this compound. The GO-EDA-BisFc provides high charge storage capacity due to the possession of both of EDLC behavior and the faradaic battery-type characteristics of GO nanosheets and Fc (as a high electroactive material), respectively. It is evident from the Fig. 8a, the CV curve area of the GO-EDA-BisFc/PANI are larger than the other samples, which may be resulting from the presence of the PANI and Fc as faradaic redox active materials in the final nanocomposite. Shorter diffusion length compared to the other samples, facilitating the diffusion and migration of the electrolyte ions and increasing charge storage capacity in the final nanocomposite. Fig. 8b illustrates the CV curves at various scan rates (10 to 200 mV/s). It can be noted that with increasing the scan rate, the peak current increases. These observations mean that the final nanocomposite has good ratability. The specific capacity, C_s (mAh g⁻¹), of the final nanocomposite at various scan rates was calculated from CV curves based on the following equation:

$$C_s = \frac{1}{3.6mv} \int_{V_a}^{V_c} I(V)dV \quad (1)$$

where I , m , and v are the current, mass of the active material, and the scan rate, respectively. The GO-EDA-BisFc/PANI nanocomposite shows specific capacities of 243.4, 239.3, 214.6, 196.7, 182.5, and 156.3 mAh g⁻¹ at a scan rate of 10, 25, 50, 75, 100, and 200 mV s⁻¹, respectively. Fig.

8c exhibits the specific capacities of the final nanocomposite at various scan rates. As shown in Fig 8c, as the scan rate increases, the specific capacity decreases. The high capacity performance at low scan rates can be attributed to the fact that the ions at low scan rates have enough time to access and penetrate into the electroactive material [66].

Additionally, the kinetic of the reaction of the final nanocomposite was analyzed via CV method at different scan rates (10 to 100 mV s^{-1}) (Fig. 9a). Generally, the current response at a fixed potential consists of two separate charge storage mechanisms including capacitive and diffusion-controlled process. The current response (i) can obey a power-law relationship with the scan rate (v) as follows (Equation 2) [67, 68]:

$$i = av^b \quad (2)$$

where a and b are the adjustable parameters. The b -value is determined from the slope of $\log i$ vs. $\log v$ as indicated in Fig. 9b. In general, slope $b=1$ assigned to the capacitive effect, while the slope $b=0.5$ corresponds to the ion diffusion-controlled process. According to this plot, the calculated b -values for all currents are close to 0.5, indicating that the charge storage mechanism of final nanocomposite is mainly controlled via ion-diffusion rather than capacitive process. Also, the contribution ratio of these two charge storage mechanisms can be calculated using the following equation:

$$i = k_1v + k_2\sqrt{v} \quad (3)$$

where k_1 and k_2 are the adjustable parameters. The first and the second parts of the Equation (3) refers to the capacitive and intercalation of ions, respectively, which can be obtained by modifying the above equation.

$$\frac{i}{\sqrt{v}} = k_1 \sqrt{v} + k_2$$

(4)

Once we know the values of k_1 and k_2 , the contribution ratio of faradaic and non-faradaic mechanisms can be easily calculated. Fig. 9c exhibits the contribution ratio of two charge storage mechanisms of the final nanocomposite vs. scan rate. As a result, faradaic contribution decreased by increasing the scan rates while non-faradaic contribution increased by increasing the scan rates. This observation might be due to electrolyte diffusion limitation at high scan rates [67, 68].

The charge storage retentions of the PANI, GO-EDA-BisFc, and GO-EDA-BisFc/PANI nanocomposite after 3000 CV cycles at a scan rate of 75 mV s^{-1} are represented in Fig.10. As shown in Fig. 10, the pure PANI and GO-EDA-BisFc show the charge storage retention of 74% (poor cycling stability) and 95% (excellent cycling stability), respectively. The swelling and shrinking of the PANI backbone during charging/discharging process can be considered as the main reason of the poor cycling stability of PANI [69]. The GO-EDA-BisFc/PANI nanocomposite shows good cycling performance (89%) compared to the pure PANI. The improving cycle life suggests a synergistic effect between modified GO nanosheets and neat PANI.

Fig. 11a represents the GCD analysis of all of the as-prepared electrodes. These experiments were performed in H_2SO_4 1 M at a current density of 2.5 A g^{-1} . As can be seen in Fig. 11a, the nearly triangular shapes of the GCD curve of GO-EDA suggest the EDLC and an ideal capacitive behavior of GO nanosheets. The GCD curves of PANI, GO-EDA-BisFc, and GO-EDA-BisFc /PANI show deviation from the regular triangular shape corresponding to the typical

redox reaction of the Fc moiety and PANI nanofibers and their faradaic battery-type effects. An important point that can be deduced from the GCD curves is the longer discharge time of the final nanocomposite compared to other materials, which may be due to the presence of Fc and PANI in the final nanocomposite structure. The presence of Fc as an electroactive material and PANI as a conducting polymer improves specific charge storage capability by increasing the rate of charge transfer and shorten ion diffusion distance for electrolyte accessibility. Fig. 11b shows the GCD curves of GO-EDA-BisFc/PANI at various current densities. An apparent increase in charge storage capacity was observed with decreasing current density. This observation reflects the fact that at high current densities the diffusion of the electrolyte ions is slow. Low diffusion of the ions leads to an incomplete insertion reaction and consequently the low specific charge storage capability.

The specific charge storage capacity C_s (in mAh g^{-1}) of the all of the as-prepared electrodes were calculated from the corresponding GCD curves via using the Equation (5):

$$C_s = \frac{i \cdot \Delta t}{m} (\text{mAh g}^{-1}) \quad (5)$$

where i is the discharging current (mA), Δt shows the discharge time (h), m denotes the mass of the active material on the working electrode (g). At a current density of 2.5 A g^{-1} , the calculated values of C_s for the PANI, GO-EDA, GO-EDA-BisFc, and GO-EDA-BisFc/PANI nanocomposites are 168, 72, 201 and 272 mAh g^{-1} , respectively. These findings, again reveals a synergistic effect between GO nanosheets, Fc, and PANI in the final nanocomposite which may lead to the observed enhanced charge storage capability. Table 1 shows a comparison between the present work and previously reported GO modified with Fc moiety electrodes. As can be seen from the table 1, the GO-EDA-BisFc/PANI nanocomposite appears to be a good candidate material for supercapacitor applications. The specific capacities of the PANI, GO-EDA, GO-

EDA-BisFc, and GO-EDA-BisFc/PANI at different current densities were depicted in Fig. 11c. Fig. 11c shows that with increasing current densities, due to the limitation of ions diffusion between electrolyte and surface of active materials, the capacity of the nanocomposites decreases. According to the Fig. 11c, the final nanocomposite possesses higher capacity compared to the other materials. Fig. 11d exhibits the cycling stability of the GO-EDA-BisFc/PANI nanocomposite after 3000 GCD cycles at 10 A g⁻¹. As indicated in Fig. 11d, the final nanocomposite possesses good cycling stability (90%). Additionally, GO-EDA-BisFc/PANI nanocomposite shows high Coulombic efficiency (CE) of ≈ 100 after 3000 GCD cycles. CE values can be calculated easily using Equation (6):

$$\eta = \frac{t_d}{t_c} \quad (6)$$

where t_c and t_d correspond to the charging and discharging time, respectively. The high CE and good cycle performance are attributed to the unique structure of the final nanocomposite.

Table 1. Comparison between this work and other reported works.

Samples	Electrolyte	Potential window (V)	Specific capacity (assumed here as battery-type pseudocapacitor) (mAh/g)	Ref.
P(FcA-co-ANI)	1M HClO ₄	-0.2 to 0.8 (Ag/AgCl)	200 at (0.5 A/g)	[70]
P(FcA-co-ANI)	1M HClO ₄	-0.2 to 0.8 (Ag/AgCl)	120 at (0.5 A/g)	[71]
CNT@TFcP/Cu	1 M H ₂ SO ₄	-0.8 to 1.4 (Ag/AgCl)	280 at (1 A/g)	[72]

GO-Fc/Mn₃O₄/PANI	1 M H ₂ SO ₄	-0.2 to 0.8 (Ag/AgCl)	233 at (2.5 A/g)	[73]
GO-PolyFc	1 M H ₂ SO ₄	-1 to 1.5 (Ag/AgCl)	139 at (2 A/g)	[39]
bA-Fc/rGO	1 M H ₂ SO ₄	-0.8 to 1.2 (Ag/AgCl)	89 at (1 A/g)	[37]
CNTs/Cs-Fc	1 M H ₂ SO ₄	-0.8 to 0.9 (Ag/AgCl)	114 at (1 A/g)	[48]
AzFc/rGO/PANI	1 M H ₂ SO ₄	-0.8 to 1.2 (Ag/AgCl)	95 at (14 A/g)	[80]
GO-B-(EtFc)- Pr3/PANI0.5	1 M H ₂ SO ₄	-0.2 to 0.8 (Ag/AgCl)	429 at (2.5 A/g)	[81]
GO-Fc/PANI	1 M H ₂ SO ₄	-0.2 to 0.8 (Ag/AgCl)	208 at (2.5 A/g)	[40]
GO-EDA- BisFc/PANI	1 M H ₂ SO ₄	-0.2 to 0.8 (Ag/AgCl)	272 at (2.5 A/g)	this work

The Nyquist plots of the GO-EDA-BisFc and GO-EDA-BisFc/PANI nanocomposite are shown in Fig. 12. The electrical equivalent circuit (EEC) used to fit the experimental data of impedance spectra and the fitting parameter are summarized in table 2. As shown in table 2, from a comparison of CPEdl-T values of GO-EDA-BisFc and GO-EDA-BisFc/PANI, it was found that the GO-EDA-BisFc/PANI nanocomposite exhibits a higher interfacial capacitance than GO-EDA-BisFc nanocomposite. These values are in agreement with results of GCD and CV analyses.

Table 2. Fitting parameters of EIS data on equivalent circuit (EEC).

Element	R_s (Ω)	CPEdl-T ($S.s^{-n}$)	CPEdl-P	R_{ct} ($\Omega.cm^2$)	W1-R	W1-T	W1-P
GO-EDA-BisFc	0.51	3.05E-6	0.98	1.27E-4	16.63	5.96E-4	0.22
GO-EDA-BisFc/PANI	0.30	5.12E-6	0.91	2.45 E-1	0.37	3.96E-5	0.26

Additionally, a symmetric supercapacitor (SSC) based on GO-EDA-BisFc/PANI nanocomposite was fabricated to evaluate final electrochemical performance of the synthesized nanocomposite. The CV curves of symmetric device at various scan rates in a maximum working potential of 1.8 V are shown in Fig. 13a. As the scan rate increasing from 10 to 50 $mV s^{-1}$, the area under CV curves increased and also the curve's shape remained unchanged. This result clearly indicates that our fabricated device exhibits good cycle life and rate capability. The GCD curves collected at different current densities (Fig. 13b). All GCD curves exhibit small ohmic drop, indicating its good rate capability. The corresponding specific capacity values calculated by Eq. 5 and the resulted plot are shown in the inset of Fig. 13b. The specific capacities were measured to 77, 73.3, 72, 66.7, and 46.7 $mAh g^{-1}$ at 1, 2, 3, 4, and 5 $A g^{-1}$, respectively. The electrochemical performance of our fabricated device and other previously reported PANI nanocomposites are shown in Ragone plot (energy density vs. power density) (Fig. 13c). The maximum energy density of 69.3 $Wh kg^{-1}$ and maximum power density of 6171 $W kg^{-1}$ for fabricated device were calculated using $E=1/2 CV$ (Eq. 7) and $P=E/\Delta t$ (Eq. 8) [74], respectively. According to the Ragone plot, our fabricated symmetric cell has the highest energy density and power density values among previously reported literature results. The Nyquist plot of symmetric supercapacitor (Fig. 13d) exhibits a smaller semicircle diameter, indicating a lower charge

transfer resistance. As shown in Fig. 13 e, after 3000 CV cycles, our fabricated device retained 86 % of initial capacitance that indicates a good cycling stability. According to the electrochemical results, our device can be regarded as potential active materials for supercapacitor applications.

4. Conclusion

In summary, we have successfully synthesized functionalized GO with bisferrocenyl based epoxy compound by ring opening reaction. Then, the PANI nanofibers adsorbed onto the modified GO surface via physical treatment to obtain the final high performance nanocomposite. The final nanocomposite was evaluated by different analyses method such as FT-IR, CV, GCD, EIS, BET, FESEM, EDX and XRD. The results showed that the presence of Fc and PANI as electroactive materials in the GO-EDA-BisFc/PANI nanocomposite control the charge storage mechanism. Therefore, the major part of the charge storage mechanism is pseudocapacitance. The GO-EDA-BisFc/PANI nanocomposite shows high discharge capacity (272 mAh g^{-1} at 2.5 A g^{-1}) and excellent capacity stability (89 %). Also, a high energy density of 69.3 Wh kg^{-1} and high power density of 6171 W kg^{-1} were achieved in a symmetrical two-electrode configuration. Based on the obtained data, it can be concluded that the GO-EDA-BisFc/PANI nanocomposite can be used as a suitable candidate in the battery-type supercapacitor applications.

Declaration of interests

The authors declare that they have no known competing financial interests or personal relationships that could have appeared to influence the work reported in this paper.

Acknowledgements

This project is supported by a research grant of the University of Tabriz (Number: SAD/796-970305).

References

1. Y. He, X. Wang, H. Huang, P. Zhang, B. Chen, Z. Guo, In-situ electropolymerization of porous conducting polyaniline fibrous network for solid-state supercapacitor, *Appl. Surf. Sci.* 469 (2019) 446-455.
2. P. Simon, Y. Gogotsi, B. Dunn, Where do batteries end and supercapacitors begin? *Science*, 343 (2014) 1210-1211.
3. H. He, L. Ma, S. Fu, M. Gan, L. Hu, H. Zhang, M. Jiang, Fabrication of 3D ordered honeycomb-like nitrogen-doped carbon/PANI composite for high-performance supercapacitors, *Appl. Surf. Sci.* 484 (2019) 1288-1296.
4. H. Yu, X. Ge, C. Bulin, R. Xing, R. Li, G. Xin, B. Zhang, Facile fabrication and energy storage analysis of graphene/PANI paper electrodes for supercapacitor application, *Electrochim. Acta*, 253 (2017) 239-247.
5. Y. Meng, K. Wang, Y. Zhang, Z. Wei, Hierarchical porous graphene/polyaniline composite film with superior rate performance for flexible supercapacitors, *Adv. Mater.* 25 (2013) 6985-6990.
6. G. Z. Chen, Supercapacitor and supercapattery as emerging electrochemical energy stores, *Int. Mater. Rev.* 62 (2016) 173-202.

7. L. L. Zhang, X. S. Zhao, Carbon-based materials as supercapacitor electrodes, *Chem. Soc. Rev.* 38 (2009) 2520-2531.
8. K. Krishnamoorthy, P. Pazhamalai, S. J. Kim, Two-dimensional siloxene nanosheets: novel high-performance supercapacitor electrode materials, *Energy & Environ. Sci.* 11 (2018) 1595-1602.
9. Z. Yu, L. Tetard, L. Zhai, J. Thomas, Supercapacitor electrode materials: nanostructures from 0 to 3 dimensions, *Energy & Environ. Sci.* 8 (2015) 702-730.
10. D. P. Dubal, O. Ayyad, V. Ruiz, P. Gomez-Romero, Hybrid energy storage: the merging of battery and supercapacitor chemistries, *Chem. Soc. Rev.* 44 (2015) 1777-1790.
11. P. Asen, S. Shahrokhian, Ternary nanostructures of Cr₂O₃/graphene oxide/conducting polymers for supercapacitor application, *J. Electroanal. Chem.* 823 (2018) 505-516.
12. J. Zhang, L. Su, L. Ma, D. Zhao, C. Qin, Z. Jin, K. Zhao, Preparation of inflorescence-like ACNF/PANI/NiO composite with three-dimensional nanostructure for high performance supercapacitors, *J. Electroanal. Chem.* 790 (2017) 40-49.
13. Y. Li, Q. Yan, Y. Wang, Y. Li, M. Zhu, K. Cheng, X. Zhang, Polyaniline coated 3D crosslinked carbon nanosheets for high-energy-density supercapacitors, *Appl. Surf. Sci.* 493 (2019) 506-513.
14. A. K. Geim, K. S. Novoselov, The rise of graphene, *Nat. Mater.* 6 (2007) 183-191.
15. D. Tian, X. Lu, G. Nie, M. Gao, N. Song, C. Wang, Growth of polyaniline thorns on hybrid electrospun CNFs with nickel nanoparticles and graphene nanosheets as binder-free electrodes for high-performance supercapacitors, *Appl. Surf. Sci.* 458 (2018) 389-396.

16. A. Ladrón-de-Guevara, Boscá, J. Pedrós, E. Climent-Pascual, A. De Andrés, F. Calle, J. Martínez, Reduced graphene oxide/polyaniline electrochemical supercapacitors fabricated by laser, *Appl. Surf. Sci.* 467 (2019) 691-697.
17. C. C. Hu, C. H. Chu, Electrochemical impedance characterization of polyaniline-coated graphite electrodes for electrochemical capacitors-effects of film coverage/thickness and anions, *J. Electroanal. Chem.* 503 (2001) 105-116.
18. K. Zhang, L. L. Zhang, X. S. Zhao, J. Wu, Graphene/polyaniline nanofiber composites as supercapacitor electrodes, *Chem. Mater.* 22 (2010) 1392-1401.
19. K. H. An, K. K. Jeon, J. K. Heo, S. C. Lim, D. J. Bae, Y. H. Lee, High-capacitance supercapacitor using a nanocomposite electrode of single-walled carbon nanotube and polypyrrole, *J. Electrochem. Soc.* 149 (2002) 1058-1062.
20. M. Li, L. Yang, Intrinsic flexible polypyrrole film with excellent electrochemical performance, *J. Mater. Sci. Mater. Electron.* 26 (2015) 4875-4879.
21. P. Asen, S. Shahrokhian, A high performance supercapacitor based on graphene/polypyrrole/ $\text{Cu}_2\text{O-Cu}(\text{OH})_2$ ternary nanocomposite coated on nickel foam, *J. Phys. Chem. C*, 121 (2017) 6508-6519.
22. M. Yan, Y. Yao, J. Wen, L. Long, M. Kong, G. Zhang, X. Liao, G. Yin, Z. Huang, Construction of a hierarchical $\text{NiCo}_2\text{S}_4@ \text{PPy}$ core-shell heterostructure nanotube array on Ni foam for a high-performance asymmetric supercapacitor, *ACS Appl. Mater. Interfaces*, 8 (2016) 24525-24535.
23. Q. Lu, Y. Zhou, Synthesis of mesoporous polythiophene/ MnO_2 nanocomposite and its enhanced pseudocapacitive properties, *J. Power Sources*, 196 (2011) 4088-4094.

24. B. H. Patil, A. D. Jagadale, C. D. Lokhande, Synthesis of polythiophene thin films by simple successive ionic layer adsorption and reaction (SILAR) method for supercapacitor application, *Synth. Met.* 162 (2012) 1400-1405.
25. Q. Chen, J. Chen, Y. Zhou, C. Song, Q. Tian, J. Xu, C. P. Wong, Enhancing pseudocapacitive kinetics of nanostructured MnO₂ through anchoring onto biomass-derived porous carbon, *Appl. Surf. Sci.* 440 (2018) 1027-1036.
26. H. Liu, B. Xu, M. Jia, M. Zhang, B. Cao, X. Zhao, Y. Wang, Polyaniline nanofiber/large mesoporous carbon composites as electrode materials for supercapacitors, *Appl. Surf. Sci.* 332 (2015) 40-46.
27. H. Qiu, X. Han, F. Qiu, J. Yang, Facile route to covalently-jointed graphene/polyaniline composite and its enhanced electrochemical performances for supercapacitors, *Appl. Surf. Sci.* 376 (2016) 261-268.
28. C. Yang, L. Zhang, N. Hu, Z. Yang, H. Wei, Z.J. Xu, Y. Wang, Y. Zhang Densely-packed graphene/conducting polymer nanoparticle papers for high-volumetric-performance flexible all-solid-state supercapacitors, *Appl. Surf. Sci.* 379 (2016) 206-212.
29. M. Naseri, L. Fotouhi, A. Ehsani, F. Babaei, Physicoelectrochemical properties of facilely electrosynthesized reduced graphene oxide/p-type conductive polymer nanocomposite film, *New J. Chem.* 40 (2016) 2565-2573.
30. A. Subramania, S. L. Devi, Polyaniline nanofibers by surfactant assisted dilute polymerization for supercapacitor applications, *Polym. Adv. Technol.* 19 (2008) 725-727.
31. J. Wang, D. Zhang, One dimensional nanostructured polyaniline: syntheses, morphology controlling, formation mechanisms, new features, and applications, *Adv. Polym. Technol.* 32 (2013) 323-368.

32. X. Zhang, W. J. Goux, S. K. Manohar, Synthesis of polyaniline nanofibers by nanofiber seeding, *J. Am. Chem. Soc.* 126 (2004) 4502-4503.
33. S. Palaniappan, P. Srinivas, Nanofibre polyaniline containing long chain and small molecule dopants and carbon composites for supercapacitor, *Electrochim. Acta*, 95 (2013) 251-259.
34. R. Teimuri-Mofrad, M. Gholamhosseini-Nazari, E. Payami, S. Esmati, Novel ferrocene-based ionic liquid supported on silica nanoparticles as efficient catalyst for synthesis of naphthopyran derivatives, *Res. Chem. Intermed.* 43 (2017) 7105-7118.
35. R. Teimuri-Mofrad, M. Gholamhosseini-Nazari, E. Payami, S. Esmati, Ferrocene-tagged ionic liquid stabilized on silica-coated magnetic nanoparticles: Efficient catalyst for the synthesis of 2-amino-3-cyano-4*H*-pyran derivatives under solvent-free conditions, *Appl. Organomet. Chem.* 32 (2018) e3955.
36. G. Divyapriya, R. Srinivasan, I. M. Nambi, J. Senthilnathan, Highly active and stable ferrocene functionalized graphene encapsulated carbon felt array-A novel rotating disc electrode for electro-Fenton oxidation of pharmaceutical compounds, *Electrochim. Acta*, 283 (2018) 858-870.
37. R. Teimuri-Mofrad, R. Hadi, H. Abbasi, Synthesis and characterization of ferrocene-functionalized reduced graphene oxide nanocomposite as a supercapacitor electrode material, *J. Organomet. Chem.* 880 (2019) 355-362.
38. R. Teimuri-Mofrad, R. Hadi, H. Abbasi, R. F. B. Baj, Synthesis, Characterization and Electrochemical Study of Carbon Nanotube/Chitosan-Ferrocene Nanocomposite Electrode as Supercapacitor Material, *J. Electron. Mater.* 48 (2019) 4573-4581.

39. R. Teimuri-Mofrad, H. Abbasi, R. Hadi, Graphene oxide-grafted ferrocene moiety via ring opening polymerization (ROP) as a supercapacitor electrode material, *Polymer*, 167 (2019) 138-145.
40. R. Teimuri-Mofrad, E. Payami, I. Ahadzadeh, Synthesis, characterization and electrochemical evaluation of a novel high performance GO-Fc/PANI nanocomposite for supercapacitor applications, *Electrochim. Acta*, 321 (2019) 134706.
41. Y. Gao, G. Hu, W. Zhang, D. Ma, X. Bao, π - π Interaction intercalation of layered carbon materials with metallocene, *Dalton Trans.* 40 (2011) 4542-4547.
42. R. Teimuri-Mofrad, K. Rahimpour, A. Aghaiepour, New ethylferrocenyl based pyranilidene bridge dyads: Synthesis, characterization and investigation of electrochemical and optical properties, *J. Organomet. Chem.* 896 (2019) 16-23.
43. G. W. Cannon, R. C. Ellis, J. R. Leal, Methyl cyclopropyl ketone, *Org. Synth.* 31 (1951) 74.
44. R. Teimuri-Mofrad, S. Esmati, S. Tahmasebi, M. Gholamhosseini-Nazari, Bisferrocene-containing ionic liquid supported on silica coated Fe_3O_4 : A novel nanomagnetic catalyst for the synthesis of dihydropyrano [2, 3-c] coumarin derivatives, *J. Organomet. Chem.* 870 (2018) 38-50.
45. A. Phillip, A. Mihai, Compounds and compositions as modulators of GPR119 activity, WO2009038974A1.
46. B. Gary, S. Renato, Chemokine receptor binding heterocyclic compounds with enhanced efficacy, US2003220341A1.
47. R. Teimuri-Mofrad, R. Alizadeh, S. Ramazani, A. R. Vaez, Preparation of Electrospun Electroactive Nanofibers of Four Arm Star-Shaped Poly (ϵ -Caprolactone)-b-Poly (2-

- Hydroxyethyl Methacrylate) and Its Blends with Polyaniline, *Polym. Plast. Technol. Eng.* 57 (2018) 893-902.
48. W. S. Hummers Jr, R. E. Offeman, Preparation of graphitic oxide, *J. Am. Chem. Soc.* 80 (1958) 1339-1339.
49. B. Xue, J. Zhu, N. Liu, Y. Li, Facile functionalization of graphene oxide with ethylenediamine as a solid base catalyst for Knoevenagel condensation reaction, *Catal. Commun.* 64 (2015) 105-109.
50. J. Gut, P. J. Rosenthal, V. Kumar, β -amino-alcohol tethered 4-aminoquinoline-isatin conjugates: Synthesis and antimalarial evaluation, *Eur. J. Med. Chem.* 84 (2014) 566-573.
51. H. Wang, Q. Hao, X. Yang, L. Lu, X. Wang, Effect of graphene oxide on the properties of its composite with polyaniline, *ACS Appl. Mater. Interfaces*, 2 (2010) 821-828.
52. L. R. Vargas, A. K. Poli, R. D. C. L. Dutra, C. B. D. Souza, M. R. Baldan, E. S. Gonçalves, Formation of Composite Polyaniline and Graphene Oxide by Physical Mixture Method, *J. Aerosp. Technol. Manag.* 9 (2017) 29-38.
53. S. Zhu, M. Wu, M. H. Ge, H. Zhang, S. K. Li, C. H. Li, Design and construction of three-dimensional CuO/polyaniline/rGO ternary hierarchical architectures for high performance supercapacitors, *J. Power Sources*, 306 (2016) 593-601.
54. L. Wang, X. Lu, S. Lei, Y. Song, Graphene-based polyaniline nanocomposites: preparation, properties and applications, *J. Mater. Chem. A*, 2 (2014) 4491-4509.
55. J. Yu, F. Xie, Z. Wu, T. Huang, J. Wu, D. Yan, C. Huang, L. Li, Flexible metallic fabric supercapacitor based on graphene/polyaniline composites, *Electrochim. Acta*, 259 (2018) 968-974.

56. Q. Zhang, Y. Li, Y. Feng, W. Feng, Electropolymerization of graphene oxide/polyaniline composite for high-performance supercapacitor, *Electrochim. Acta*, 90 (2013) 95-100.
57. B. Zawisza, A. Baranik, E. Malicka, E. Talik, R. Sitko, Preconcentration of Fe (III), Co (II), Ni (II), Cu (II), Zn (II) and Pb (II) with ethylenediamine-modified graphene oxide. *Microchim. Acta*, 183 (2016) 231-240.
58. A.G. Tabrizi, N. Arsalani, A. Mohammadi, L.S. Ghadimi, I. Ahadzadeh, H. Namazi, A new route for the synthesis of polyaniline nanoarrays on graphene oxide for high-performance supercapacitors, *Electrochim. Acta*, 265 (2018) 379-390.
59. M. Wang, G. Ji, B. Zhang, D. Tang, Y. Yang, Y. Du, Controlled synthesis and microwave absorption properties of Ni_{0.6}Zn_{0.4}Fe₂O₄/PANI composite via an in-situ polymerization process, *J. Magn. Mater.* 377 (2015) 52-58.
60. L. Shi, X. Wang, L. Lu, X. Yang, X. Wu, Preparation of TiO₂/polyaniline nanocomposite from a lyotropic liquid crystalline solution, *Synth. Met.* 159 (2009) 2525-2529.
61. S. Bose, T. Kuila, M. E. Uddin, N. H. Kim, A. K. Lau, J. H. Lee, In-situ synthesis and characterization of electrically conductive polypyrrole/graphene nanocomposites, *Polymer*, 51 (2010) 5921-5928.
62. Z.-F. Li, H. Zhang, Q. Liu, Y. Liu, L. Stanciu, J. Xie, Covalently-grafted polyaniline on graphene oxide sheets for high performance electrochemical supercapacitors, *Carbon*, 71 (2014) 257-267.
63. V. Gedela, S. K. Puttapati, C. Nagavolu, V.V. S. S. Srikanth, A unique solar radiation exfoliated reduced graphene oxide/polyaniline nanofibers composite electrode material for supercapacitors, *Mater. Lett.* 152 (2015) 177-180.

64. D. Xu, Q. Xu, K. Wang, J. Chen, Z. Chen, Fabrication of free-standing hierarchical carbon nanofiber/graphene oxide/polyaniline films for supercapacitors, *ACS Appl. Mater. Interfaces*, 6 (2014) 200-209.
65. J. Yan, T. Wei, B. Shao, Z. Fan, W. Qian, M. Zhang, F. Wei, Preparation of a graphene nanosheet/polyaniline composite with high specific capacitance, *Carbon*, 48 (2010) 487-493.
66. S. Vijayakumar, S. Nagamuthu, K.S. Ryu, CuCo_2O_4 flowers/Ni-foam architecture as a battery type positive electrode for high performance hybrid supercapacitor applications, *Electrochim. Acta*, 238 (2017) 99-106.
67. Y. Dou, Y. Wang, D. Tian, J. Xu, Z. Zhang, Q. Liu, B. Ruan, J. Ma, Z. Sun, S.X. Dou, Atomically thin Co_3O_4 nanosheet-coated stainless steel mesh with enhanced capacitive Na^+ storage for high-performance sodium-ion batteries, *2D Material*, 4 (2017) 015022.
68. S. Loua, X. Cheng, Y. Zhao, A. Lushington, J. Gao, Q. Li, P. Zuo, B. Wang, Y. Gao, Y. Ma, C. Du, G. Yin, X. Sun, Superior performance of ordered macroporous TiNb_2O_7 anodes for lithium ion batteries: understanding from the structural and pseudocapacitive insights on achieving high rate capability, *Nano Energy* 34 (2017) 15-25.
69. M.A. Deyab, G. Mele, PANI@ Co-Porphyrins composite for the construction of supercapacitors, *J. Energy Storage*, 26 (2019)101013.
70. Y. Li, Y. Zheng, Preparation of a P (FcA-co-ANI)/graphene composite for application in supercapacitors, *High Perform. Polym.* 29 (2017) 524-532.
71. Y. Li, Y. Zheng, Synthesis and characterization of a ferrocene-modified, polyaniline-like conducting polymer, *J. Appl. Polym. Sci.* 133 (2016) 43217.

72. R. Teimuri-Mofrad, R. Hadi, H. Abbasi, E. Payami, S. Neshad, Green synthesis of carbon nanotubes@tetraferrocenylporphyrin/copper nanohybrid and evaluation of its ability as a supercapacitor, *J. Organomet. Chem.* 899 (2019) 120915.
73. E. Payami, A. Aghaiepour, K. Rahimpour, R. Mohammadi, R. Teimuri-Mofrad, Design and synthesis of ternary GO-Fc/Mn₃O₄/PANI nanocomposite for energy storage applications, *J. Alloys Compd.* (2020) 154485.
74. L. Deng, Z. Ma, Z.H. Liu, G. Fan, Battery-type graphene/BiOBr composite for high-performance asymmetrical supercapacitor, *J. Alloys Compound.* 812 (2020) 152087.
75. V. Sahu, R. B. Marichi, G. Singh, R. K. Sharma, Hierarchical polyaniline spikes over vegetable oil derived carbon aerogel for solid-state symmetric/asymmetric supercapacitor, *Electrochim. Acta*, 240 (2017) 146-154.
76. M. N. Rantho, M. J. Madito, N. Manyala, Symmetric supercapacitor with supercapattery behavior based on carbonized iron cations adsorbed onto polyaniline, *Electrochim. Acta*, 262 (2018) 82-96.
77. S. Palaniappan, P. Srinivas, Nano fibre polyaniline containing long chain and small molecule dopants and carbon composites for supercapacitor, *Electrochim. Acta*, 95 (2013) 251-259.
78. A. Shanmugavani, S. Kaviselvi, K.V. Sankar, R.K. Selvan, Enhanced electrochemical performances of PANI using redox additive of K₄ [Fe (CN) ₆] in aqueous electrolyte for symmetric supercapacitors, *Mater. Res.* 62 (2015)161-167.
79. L.S. N. Ghadimi, A. G. Arsalani, Tabrizi, A. Mohammadi, I. Ahadzadeh, Novel nanocomposite of MnFe₂O₄ and nitrogen-doped carbon from polyaniline carbonization as electrode material for symmetric ultra-stable supercapacitor, *Electrochim. Acta*, 282 (2018)116-127.

80. R. Hadi, H. Abbasi, E. Payami, I. Ahadzadeh, R. Teimuri-Mofrad, Synthesis, Characterization and Electrochemical Properties of 4- Azidobutylferrocene- Grafted Reduced Graphene Oxide- Polyaniline Nanocomposite for Supercapacitor Applications, *Chem. Select*, 5(2020) 575-583.
81. E. Payami, I. Ahadzadeh, R. Mohammadi, R. Teimuri-Mofrad, Design and synthesis of novel binuclear ferrocenyl-intercalated graphene oxide and polyaniline nanocomposite for supercapacitor applications, *Electrochim. Acta*, 342 (2020) 136078.

Figures captions:

Fig. 1. The CV curve of BisFc-Epo in a conventional three-electrode system (GC as working electrode, Ag/AgCl as reference electrode, and Pt wire as counter electrode) in the 0.1 M LiClO₄ in acetonitrile at 50 mV s⁻¹.

Fig. 2. The possible interactions between final nanocomposite components including Fc rings, GO nanosheets and PANI nanofibers.

Fig. 3. The FT-IR spectra of the BisFc-Epo, PANI, GO, GO-EDA, GO-EDA-BisFc, GO-EDA-BisFc/PANI nanocomposite in the range of 400-4000 cm⁻¹.

Fig. 4. FE-SEM graphs of the (a) PANI, (b) GO, (c) GO-EDA, (d) GO-EDA-BisFc, (e & f) GO-EDA-BisFc/PANI nanocomposite.

Fig. 5. The EDX curves of (a) PANI, (b) GO, (c) GO-EDA, (d) GO-EDA-BisFc, (e) GO-EDA-BisFc/PANI nanocomposite.

Fig. 6. The XRD patterns of GO (inset), PANI, GO-EDA, GO-EDA-BisFc, and GO-EDA-BisFc/PANI nanocomposite.

Fig. 7. N₂ adsorption/desorption isotherms and their BJH pore size distribution (inset) of GO-EDA-BisFc and GO-EDA-BisFc/PANI nanocomposites.

Fig. 8. (a) CV diagrams of GO, PANI, GO-EDA-BisFc, and GO-EDA-BisFc /PANI electrodes in three-electrode system at a scan rate of 50 mV s⁻¹ in H₂SO₄ 1M, (b) CV diagrams of the GO-EDA-BisFc /PANI electrode at different scan rates ranging from 10 to 200 mV s⁻¹, (c) specific capacities of the GO-EDA-BisFc /PANI at various scan rates ranging from 10 to 200 mV s⁻¹.

Fig. 9. (a) CV diagrams of GO-EDA-BisFc /PANI electrode at various scan rates ranging from 10 to 100 mV s^{-1} (b) linear plot between $\log i$ vs. $\log v$, (c) faradaic and non-faradaic contribution of the final nanocomposite at various scan rates.

Fig. 10. The charge storage retention plots of PANI, GO-EDA-BisFc, and GO-EDA-BisFc /PANI after 3000 CV cycles at 75 mV s^{-1} in H_2SO_4 1M.

Fig. 11. (a) GCD plots of all electrodes at 2.5 A g^{-1} in H_2SO_4 1M, (b) GCD plots of GO-EDA-BisFc/PANI nanocomposite at different current densities ranging from 2.5 to 10 A g^{-1} , (c) Specific capacity of PANI, GO-EDA, GO-EDA-BisFc, and GO-EDA-BisFc/PANI nanocomposite at different current densities, (d) the cycling stability and CE of GO-EDA-BisFc/PANI nanocomposite after 3000 GCD cycles at 10 A g^{-1} .

Fig. 12. Nyquist diagrams of the GO-EDA-BisFc and GO-EDA-BisFc/PANI nanocomposites.

Fig. 13. (a) CV curves of fabricated device at different scan rates ranging from 10 to 50 mV s^{-1} , (b) GCD curves at different current densities ranging from 1 to 5 A g^{-1} and inset: Specific capacity values, (c) Ragone plot, (d) Nyquist plot of fabricated device, and (e) The charge storage retention plots of fabricated device after 3000 CV cycles at 75 mV s^{-1} .

Schemes captions:

Scheme 1. Preparation process of BisFc-Epo.

Scheme 2. Functionalization process of the GO nanosheets.

Scheme 3. The preparation process of the final nanocomposite.

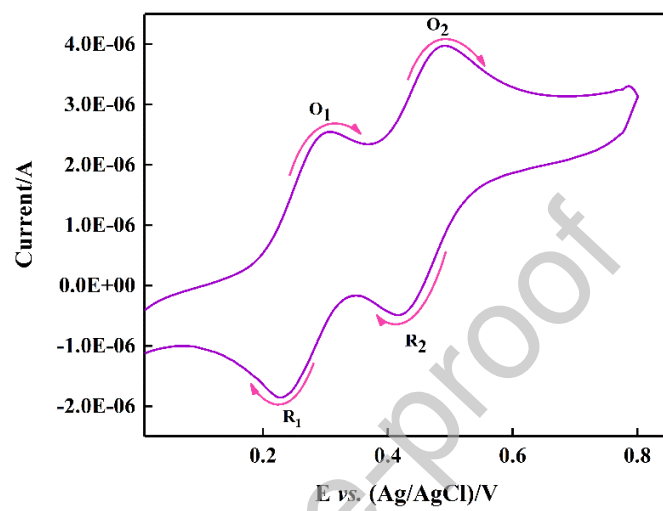


Fig. 1

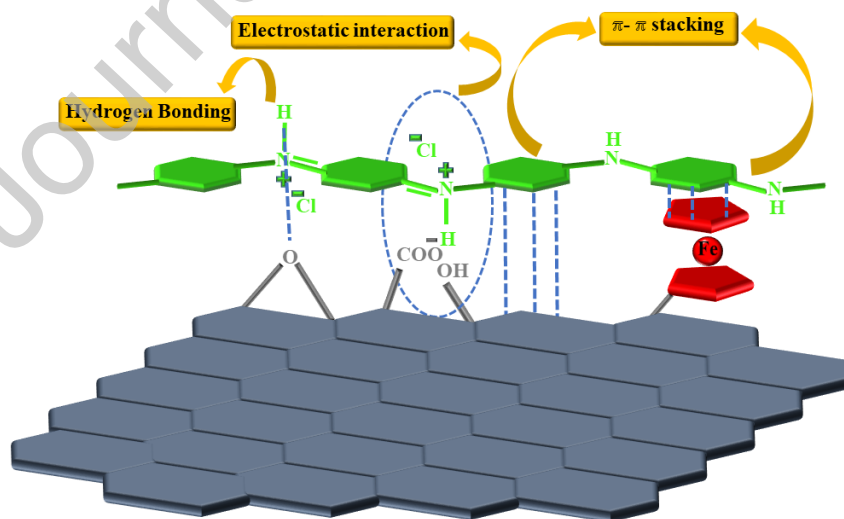


Fig. 2

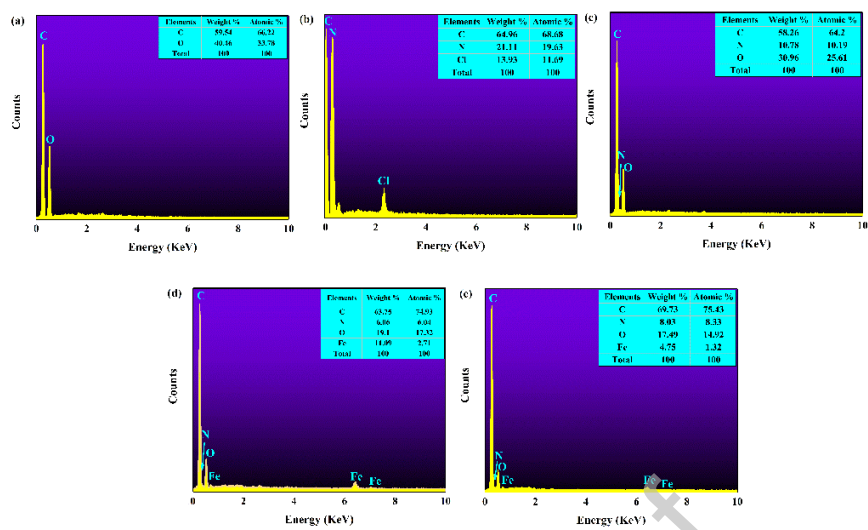


Fig. 5

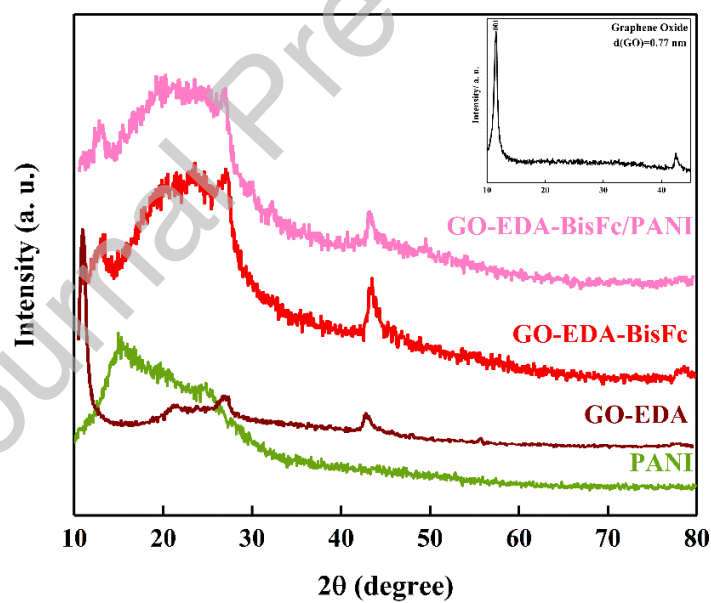


Fig. 6

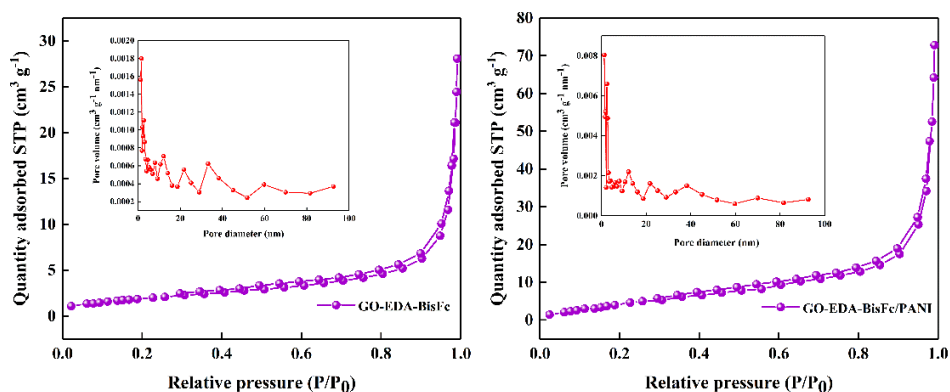


Fig. 7

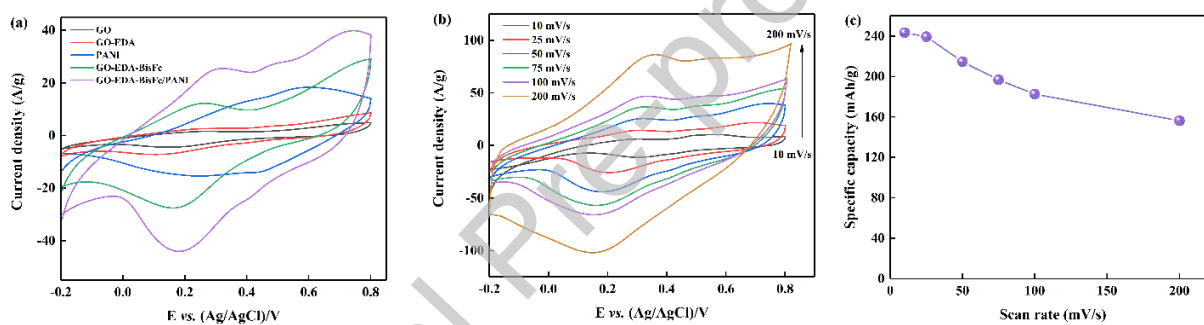


Fig. 8

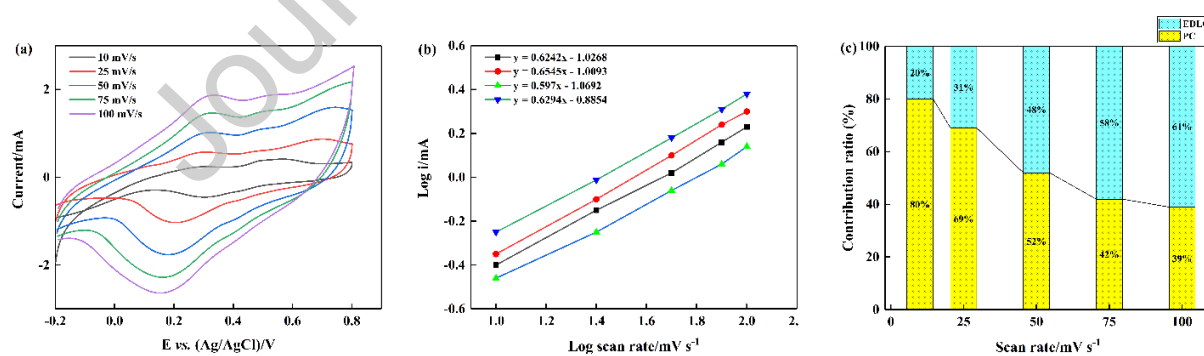


Fig. 9

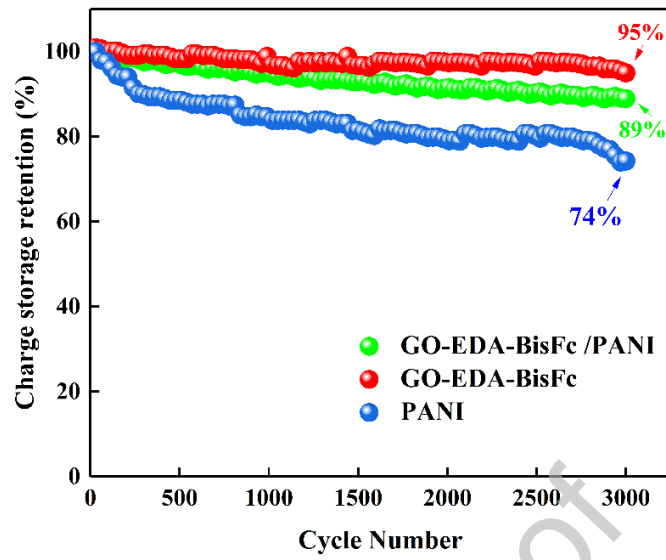


Fig. 10

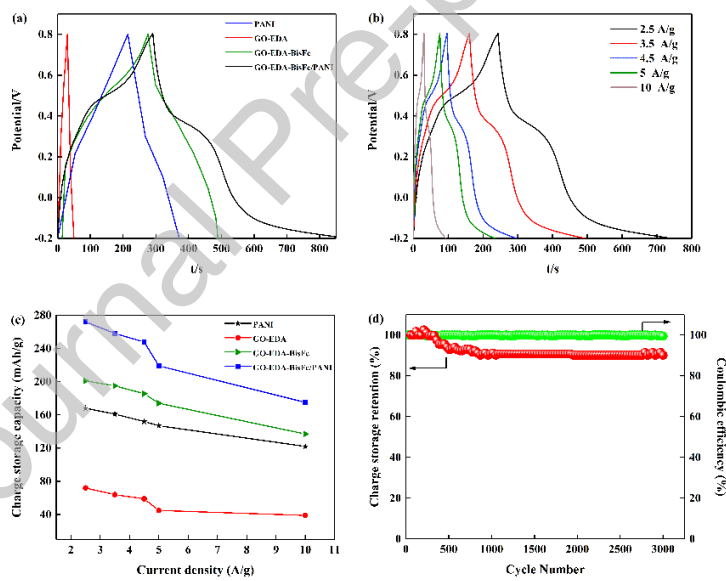


Fig. 11

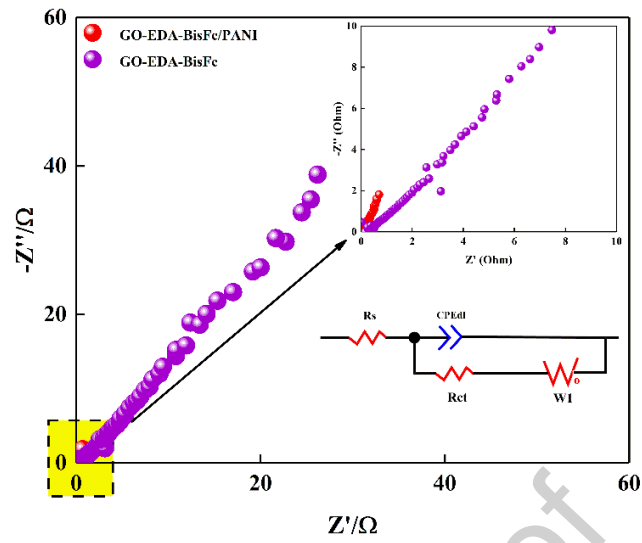


Fig. 12

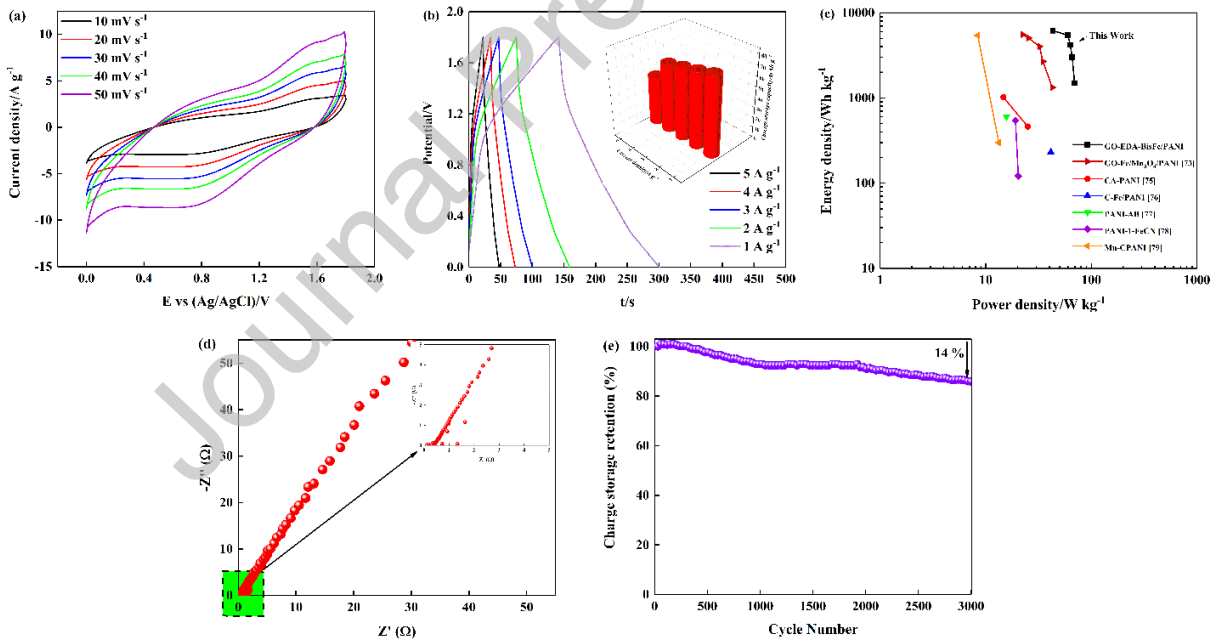
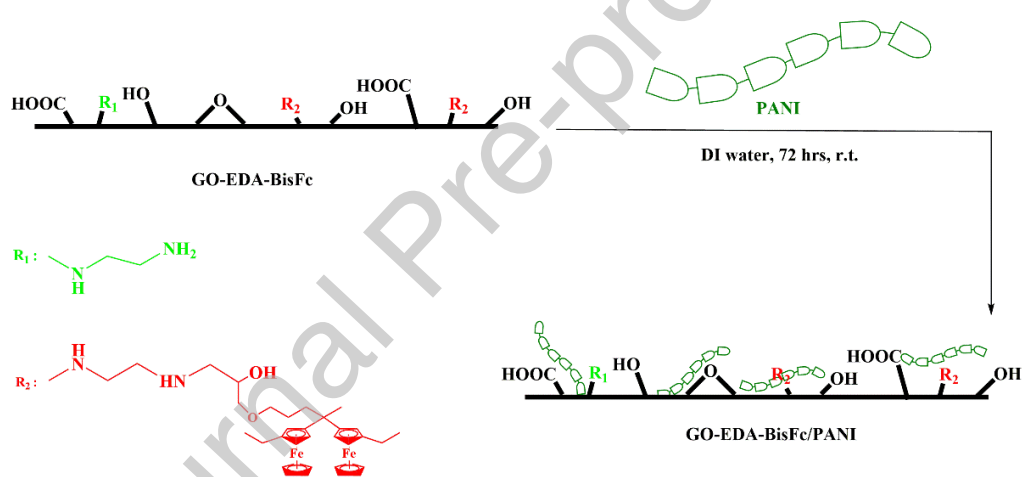
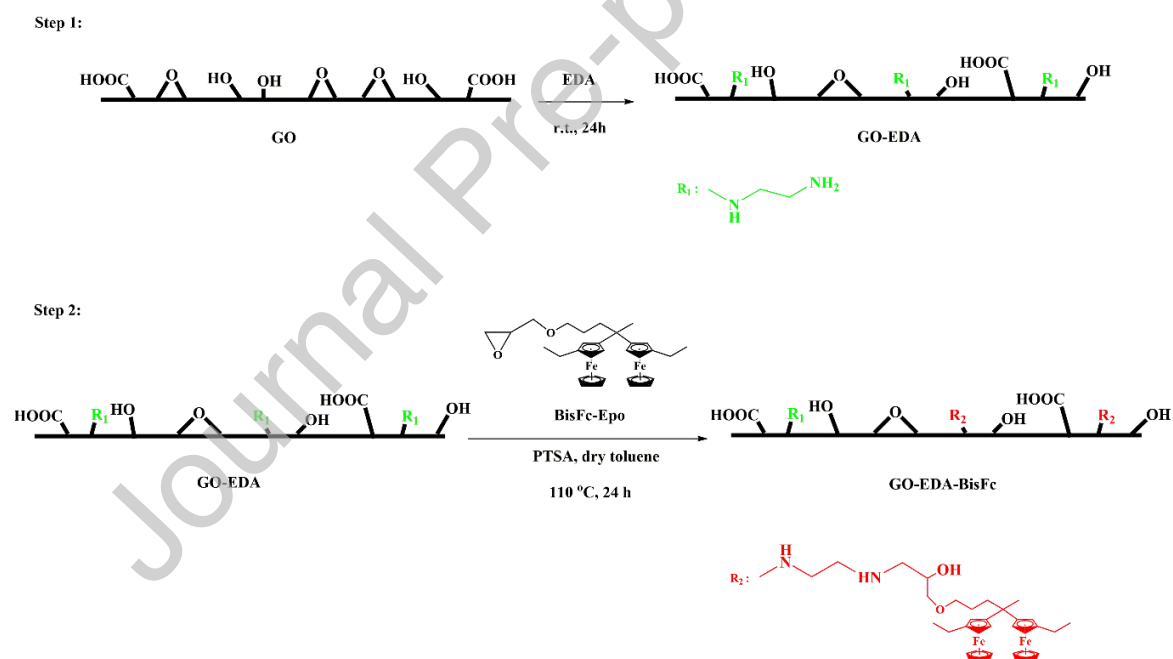
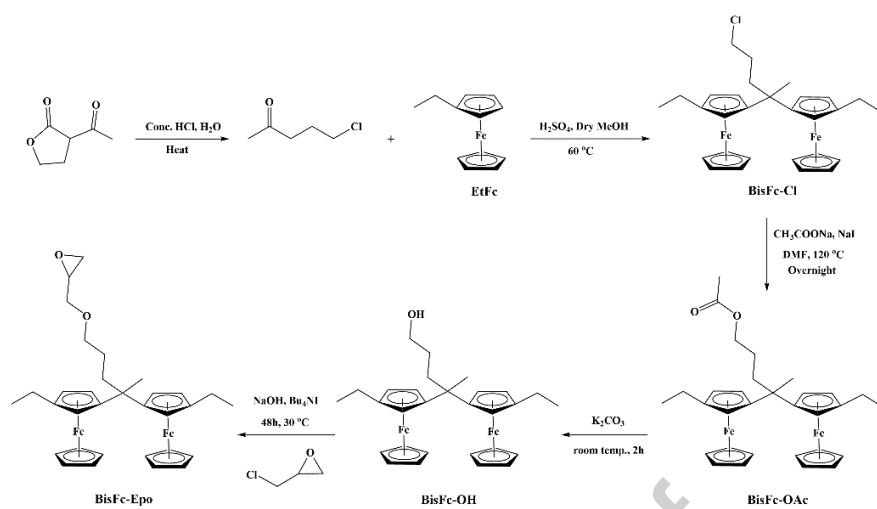


Fig. 13



Scheme 1



Graphical Abstract

